A theoretical study on throttle ranges of O/F controllable hybrid rocket propulsion systems

Kohei OZAWA* and Toru SHIMADA**
* Department of Mechanical and Control Engineering, Kyushu Institute of Technology
1-1, Sensui-cho, Tobata-ku, Kitakyushu city, Fukuoka 804-8550, Japan
E-mail: ozawa.kohei582@mail.kyutech.jp
**Department of Space Flight Engineering, Institute of Space and Astronautical Science, Japan Aerospace Exploration Agency
3-1-1, Yoshinodai, Chuo-ku, Sagamihara city, Kanagawa 252-5210, Japan

Received: XXXX; Revised: XXXX; Accepted: XXXX

Abstract
The characteristics of several O/F control methods for hybrid rocket propulsion have been discussed and theoretically analyzed from the physical properties of propellants and fuel regression behavior. In this research, comparisons have been made among different oxidizer injection methods of Altering-intensity Swirling Oxidizer Flow Type (A-SOFT), Aft-chamber Oxidizer Injection Method (AOIM), and Swirling-AOIM for the throttle range with a constant O/F, design restrictions of the fuel grain, penalties on the adoption of the methods, and suitable scales of the engine. Theoretical analysis on regression rates has revealed that A-SOFT has upper and lower limits of throttle while maintaining a constant O/F whereas AOIM does not have any lower limit, and Swirling-AOIM covers both the throttle ranges. The designing restriction of the fuel grain derived from the regression rate behavior has indicated that A-SOFT using paraffin and oxygen has a potential to maintain 50-100% throttle range over a burn. The penalties for the adoption of these O/F control methods have also been discussed from the aspects of the increase in the complexity of the system, structural mass, and pressure drop at the injector for the methods using gaseous injection. The pressure drop has quantitatively been evaluated by relating the available swirl strength with the cross-sectional area and gaseous oxidizer mass flux at the injector. This analysis has revealed 5 times difference in the available swirl strength between the gaseous oxygen and the decomposed gas of 90% hydrogen peroxide. The sizing of the 1st stage of the satellite launcher has revealed that A-SOFT and Swirling-AOIM are suitable for small-scale engines with a propellant mass of 10^0-10^2 [ton] using paraffin and liquid oxygen whereas AOIM and Swirling-AOIM are suitable for engines with paraffin and 90% hydrogen peroxide.

Keywords : Hybrid rockets, mixture ratio control, swirling flow, conceptual design of rockets.

1. Introduction

O/F shifts in hybrid rockets are phenomena causing shifts in unit mass enthalpy of the productive gases from the engine (Waidmann, 1988), (Altman, 1995), but historically the performance drops due to such shifts have been evaluated as a negligible loss. However, recent researches have revealed that residual mass of unused propellants due to O/F shifts is an overlooked factor that decreases the flight performance. The current research (Ozawa and Shimada, 2017) revealed that residuals due to the random or systematic uncertainty of fuel regression rates also decrease flight performance in addition to shifts in enthalpy observed in O/F shifts along nominal fuel regression behaviors. In particular, the random uncertainty of fuel regression rates decreases the 3σ limit of the flight performance. Usuki and Shimada (2015) performed the optimization of a conceptual design of sounding hybrid rockets for a multipurpose mission to maintain a constant hovering altitude and time. They revealed that the residual mass of propellants decreases the flight performance of the conventional hybrid rocket with O/F shifts when the hovering duration is prioritized.

Technologies to eliminate O/F shifts have already been proposed in the past. Aft-end Oxidizer Injection Method (AOIM) and Altering-intensity Swirling Oxidizer Flow Type hybrid rockets (A-SOFT) are two such representative

Paper No.xx-xxxx (This paper is based on the paper in the proceedings of xxxxx Conference (20xx), No.xxx.)
[DOI: 10.1299/xxx.2017xxx000x]

technologies. The concept of AOIM is to adjust O/F ratio by adding oxidizer mass flow rates from the aft-chamber as is shown in Fig. 1. This type of O/F control has been proposed by Boardman et al. (1995), but it is not clear whether an experimental demonstration was actually performed. Recently, A-SOFT has been proposed as another type of O/F control method by Ozawa and Shimada (2015). The concept of A-SOFT is to control swirl number of the oxidizer in addition to total mass flow rate of the oxidizer applying the dependence of the swirl number on fuel regression rates (Tamura et al., 1999). This concept has been demonstrated by static burn experiments (Ozawa et al., 2016).

The practical suitability of these O/F control methods depends on the scale of engines, the selected propellants, throttle range, engine cycles, and structural mass penalties due to the introduction of such technologies. The purpose of this study is to discuss the suitability, advantages, and disadvantages of these methods for several scales of the engine and combinations of propellants. This article discusses the theoretical throttle ranges where the individual technologies can eliminate O/F shifts. We also classify the risk factors causing the structural mass penalties by adopting each method from the viewpoint of propulsion systems. In the second part, this article quantitatively evaluates one of these risk factors, the pressure drop at the injector to obtain the geometric swirl number, using a constraint to the geometric swirl number from the cross-sectional area of the injector, chamber pressure, and regression rate behavior. In the final part of this article, we evaluate the effective densities of the propellants and lower throttle limits for each method in various scales, initial acceleration and propellant options. The methodologies developed in this study will contribute to design optimizations and flight simulations of hybrid rockets with an O/F control capability.

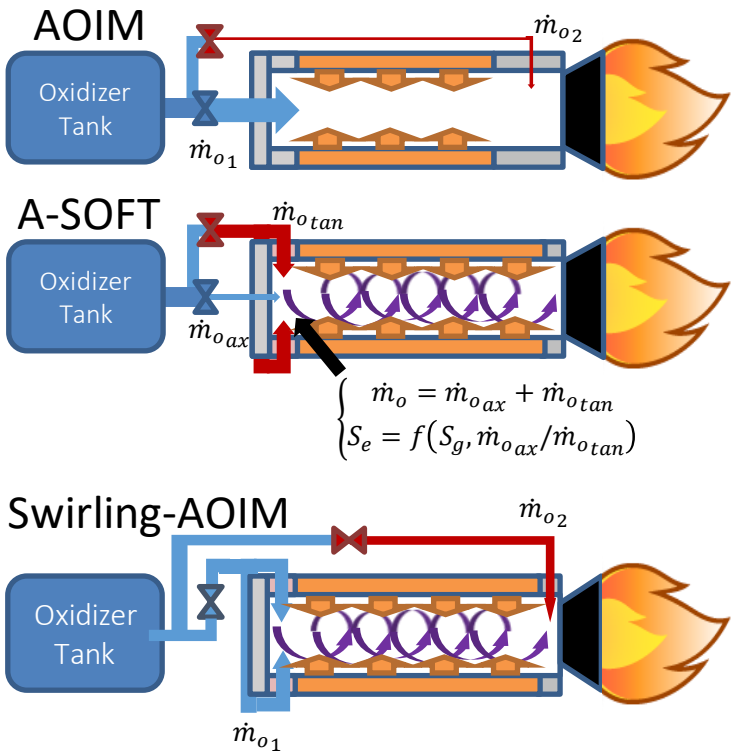

Fig. 1 Concepts of AOIM (top), A-SOFT (center), and Swirling-AOIM (bottom).

2. Theoretical throttle range of O/F control methods

In this section, the theoretical operating regions available at a constant O/F are discussed geometrically for AOIM, A-SOFT, and AOIM using swirling injection (designated as “Swirling-AOIM”). Geometric discussion makes it easy to understand the relationships among the operating regions of these three methods.

2.1 AOIM

AOIM is one of the simplest ideas to eliminate O/F shifts by adding oxidizer to the fuel-rich burnt gas at the aft-

[DOI: 10.1299/xxx.2017xxx000x]

chamber of the engine. The advantage of this method is that the oxidizer added at the aft-chamber does not affect the regression rate of the fuel. This characteristic enables one to apply a simple feedback control law for O/F control. However, this method also has a disadvantage. The aft-chamber to inject the oxidizer into the burnt gas would further increase the length of the engine and the aspect ratio of the rocket, though the larger aspect ratios of rockets due to the low regression rates in hybrid motors has been a critical problem throughout the history of hybrid rocket propulsion.

The operating regions of propellant mass flow rate and O/F in AOIM at an arbitrary time during a burn can be geometrically expressed on a two-dimensional plane of fuel and oxidizer mass flow rates. The oxidizer mass flow rate injected from the head-end of the main chamber $\dot{m}_{o_1}$ [kg/s] and that done from the aft-chamber $\dot{m}_{o_2}$ [kg/s] are as shown in Fig.1. In AOIMs, only $\dot{m}_{o_1}$ contributes to fuel regression. These two variables are assumed to have a restriction of total oxidizer mass flow rates as

$$\begin{cases} \dot{m}_o = \dot{m}_{o_1} + \dot{m}_{o_2} \leq \dot{m}_{o_{max}} \\ \dot{m}_{o_1}, \dot{m}_{o_2} \geq 0 \end{cases} \quad (1).$$

For an AOIM with axial oxidizer injection, the conventional fuel regression rate behavior (Marxman et al., 1963) is assumed as,

$$\dot{r} = a{G_o}^n \quad (2)$$

where G_o [kg/(m^{2}s)] is the oxidizer mass flux in the fuel port, and a [kg^{-n}m^{1+2n}s^{n-1}] and n [-] are constant coefficient and oxidizer mass flux exponent, respectively. Regression rate $\dot{r}$ is expressed in [m/s]. Let us assume a single port fuel grain at any time during the burn, with a density ρ_f [kg/m^3], with r_i [m/s] as inner diameter and L_f [m] as length. Under a constant $\dot{m}_o$, the fuel mass flow rate $\dot{m}_f$ [kg/s] ranges within

$$0 \leq \dot{m}_f = 2\pi^{1-n} L_f r_i^{1-2n} \rho_f a {\dot{m}_{o_1}}^n \leq 2\pi^{1-n} L_f r_i^{1-2n} \rho_f a {\dot{m}_o}^n \quad (3).$$

Equations (1) and (3) enable us to describe the operating region on the 2-D plane of fuel and oxidizer mass flow rates as shown in Fig. 2. The light gray region and black curve on the border of the region refer to the available operating conditions of the AOIM. The black curve also refers to the fuel mass flow rate behavior of the solid fuel grain when $\dot{m}_{o_2} = 0$. The black line refers to a constant O/F. The throttle range at a constant O/F [-] is theoretically between the two cross points of the black curve and line:

$$0 \leq \dot{m}_o \leq \left(2\pi^{1-n} L_f r_i^{1-2n} \rho_f a O/F\right)^{\frac{1}{1-n}} \quad (4).$$

This result means that AOIM does not have the theoretical lower limit of throttling, and the upper limit depends on the geometry of the fuel grain and the regression rate behavior of the solid fuel.

We can easily understand that the available throttle range depends on the inner diameter $2r_i$ of the fuel grain from the right hand of Eq. (4). Because the exponent n typically ranges between 0.5 and 0.8 in conventional solid fuels, r_i^{1-2n} decreases with increasing inner port diameter. Under the assumption that the fuel grain burns out without residuals at the end of the burn, the throttle range available over the burn is

$$0 \leq \dot{m}_o \leq \left(2\pi^{1-n} L_f r_o^{1-2n} \rho_f a O/F\right)^{\frac{1}{1-n}} \quad (5)$$

where r_o [m] refers to the outer radius of the fuel grain.

[DOI: 10.1299/xxx.2017xxx000x]

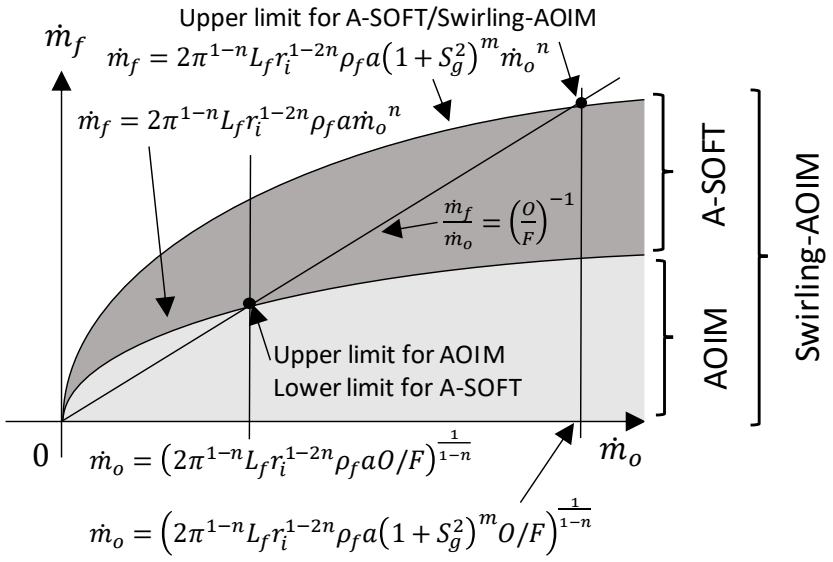

Fig. 2 Operating regions of AOIM, A-SOFT, and Swirling-AOIM with an inner diameter of $2r_i$ at arbitrary time during a burn.

2.2 A-SOFT

The concept of A-SOFT is to control both thrust and O/F by changing swirl strength of oxidizer in Swirling Oxidizer Flow Type (SOFT) hybrid rocket engines, which was originally intended to only increase regression rates. The swirl strength is independently controlled by the axially and tangentially injected oxidizer mass flow rates. A-SOFT is characterized by the contribution of both the axial and tangential oxidizer mass flow rates to fuel regression. This characteristic provides larger regression rates of SOFT and A-SOFT than those of conventional hybrids using axial injection. This advantage becomes large with the increasing scale of the rocket and gives a flexibility to the engine design and the solid fuel selection during the development. However, the need of two operating parameters for the regression rate can be a disadvantage. The increase in the freedom of the operating parameters should increase the complexity of the fuel regression rate behavior, leading to a large number of firing tests in the practical development of the engine. Moreover, the reproducibility and stability of the regression rate of A-SOFT on the two operating parameters have not been completely explored yet.

The relation between the swirl strength and regression rates in SOFT has been revealed by Tamura et al. (1999), and its fuel regression data have been collected for various scales of thrust (Shimada et al., 2017). A similar tendency has been observed also in A-SOFT by Ozawa et al. (2016). The fuel regression rate of A-SOFT is modeled as

$$\dot{r} = a(1 + S_e^2)^m G_o{}^n \tag{6}$$

where S_e [-] and m [-] refer to effective geometric swirl number and swirl number exponent, respectively. S_e is an extension of geometric swirl number, which is an evaluation parameter of swirl strength only determined from the tangential injector design. S_e is determined as the ideal angular moment normalized by the radius of the pre-chamber and the ideal axial moment of the oxidizer. Figure 3 shows a typical design of A-SOFT and the dual injector consisting of axial and tangential injectors. In this design, the oxidizer is axially injected from the 8 axial injector ports and tangentially injected from the $n_i = 8$ [-] slits with thickness dr [m] by t [m] in radial and axial directions, respectively. These oxidizer flows are combined in the pre-chamber of D [m] diameter. Provided that the oxidizer is injected at the mass flow rates $\dot{m}_{o_{ax}}$ [kg/s] and $\dot{m}_{o_{tan}}$ [kg/s] from the axial and tangential injectors, respectively, S_e under the condition should be

[DOI: 10.1299/xxx.2017xxx000x]

$$S_e = \frac{\frac{(D-dr)\dot{m}_{o_{tan}}^{\ 2}}{2 \quad n_i \rho_o dr t}}{\frac{D}{2}\frac{(\dot{m}_{o_{ax}}+\dot{m}_{o_{tan}})^2}{\rho_o \pi D^2/4}} = \frac{D(D-dr)}{n_i dr t}\frac{1}{(1+\dot{m}_{o_{ax}}/\dot{m}_{o_{tan}})^2} = \frac{S_g}{(1+\dot{m}_{o_{ax}}/\dot{m}_{o_{tan}})^2} \tag{7}$$

where ρ_o [kg/m^3] and S_g [-] refer to the density of oxidizer and the geometric swirl number of the tangential injector. This equation shows that effective geometric swirl number S_e depends only on geometric swirl number of the tangential injector S_g and the axial-tangential mass flow rate ratio $\dot{m}_{o_{ax}}/\dot{m}_{o_{tan}}$. It is clear that the available range of S_e in A-SOFT is theoretically shown as

$$0 \le S_e \le S_g \tag{8}.$$

Practically, the control range of S_e also depends on the control valves to regulate $\dot{m}_{o_{ax}}$ and $\dot{m}_{o_{tan}}$.

Let us discuss the operating region of an A-SOFT hybrid rocket engine using a solid fuel grain with the same dimension and material assumed in 2.1. The limitation of the oxidizer mass flow rates from the dual injector is assumed to be as

$$\begin{cases} \dot{m}_o = \dot{m}_{o_{ax}} + \dot{m}_{o_{tan}} \le \dot{m}_{o_{max}} \\ \dot{m}_{o_{ax}}, \dot{m}_{o_{tan}} \ge 0 \end{cases} \tag{9}.$$

Under a constant total oxidizer mass flow rate $\dot{m}_o$, the fuel mass flow rate $\dot{m}_f$ ranges

$$2\pi^{1-n} L_f r_i^{1-2n} \rho_f a \dot{m}_o^n \le \dot{m}_f \le 2\pi^{1-n} L_f r_i^{1-2n} \rho_f a \left(1+S_g^2\right)^m \dot{m}_o^n \tag{10}.$$

Figure 2 shows the operating region of A-SOFT obtained using Eq. (10). The lower and upper black curves on the border of the region are the fuel mass flow rate for $S_e = 0$ and $S_e = S_g$, respectively. The curves and the dark gray region are the operating region of the A-SOFT. The black line refers to a constant O/F. The two regions have a common border of the regression rate curve for the axial injection as shown in Fig. 2. For A-SOFT, the throttle range at the constant O/F can be expressed as

$$\left(2\pi^{1-n} L_f r_i^{1-2n} \rho_f a O/F\right)^{\frac{1}{1-n}} \le \dot{m}_o \le \left(2\pi^{1-n} L_f r_i^{1-2n} \rho_f a O/F\right)^{\frac{1}{1-n}} \left(1+S_g^2\right)^{\frac{m}{1-n}} \tag{11}.$$

The upper and lower limits of Eq. (11) depend on the fuel port radius. The throttle range available with the constant O/F over the burn is expressed as

$$\left(2\pi^{1-n} L_f r_I^{1-2n} \rho_f a O/F\right)^{\frac{1}{1-n}} \le \dot{m}_o \le \left(2\pi^{1-n} L_f r_o^{1-2n} \rho_f a O/F\right)^{\frac{1}{1-n}} \left(1+S_g^2\right)^{\frac{m}{1-n}} \tag{12}$$

where r_I [m] refers to the initial fuel port radius. This inequality gives a useful design requirement of the solid fuel grain. Provided with a throttle range between $\dot{m}_{o_{min}}$ and $\dot{m}_{o_{max}}$with a constant O/F over the burn, Eq. (12) requires

$$\begin{cases} \dot{m}_{o_{min}} \ge \left(2\pi^{1-n} L_f r_I^{1-2n} \rho_f a O/F\right)^{\frac{1}{1-n}} \\ \dot{m}_{o_{max}} \le \left(2\pi^{1-n} L_f r_o^{1-2n} \rho_f a O/F\right)^{\frac{1}{1-n}} \left(1+S_g^2\right)^{\frac{m}{1-n}} \end{cases} \tag{13}.$$

This relation can be summarized into the following design requirement,

$$1 \le \frac{r_o}{r_I} \le \left(1+S_g^2\right)^{\frac{m}{2n-1}} \left(\frac{\dot{m}_{o_{min}}}{\dot{m}_{o_{max}}}\right)^{\frac{1-n}{2n-1}} \tag{14}.$$

Under this requirement, the maximum packing density of the fuel grain is,

[DOI: 10.1299/xxx.2017xxx000x]

$$1-\left(\frac{r_o}{r_l}\right)^{-2}=1-\left(1+S_g^2\right)^{\frac{-2m}{2n-1}}\left(\frac{\dot{m}_{o_{min}}}{\dot{m}_{o_{max}}}\right)^{\frac{-2(1-n)}{2n-1}} \quad (15).$$

Figure 4 shows the relation between the lower throttle limit and the upper limit of the packing density based on Eq. (15). The exponents of polypropylene and gaseous oxygen: $m=0.0987$ and $n=0.651$, which were the result in the firing experiments of A-SOFT (Ozawa et al., 2016), are substituted in this figure. This figure allows us to understand that polypropylene and gaseous oxygen can easily achieve a throttlability of 50% over the burn, but it is difficult to achieve a broader throttle range over the burn. A tangential injector with $S_g \geq 20$ enables 50% throttle rate over the burn with a packing density larger than 90%. However, 20% throttle over the burn with a packing density larger than 70% requires S_g larger than 40.

2.3 Swirling-AOIM

Swirling-AOIM is defined as a type of AOIM using swirling oxidizer injection at the head-end of the engine as shown in Fig. 2. This method is intended to cover all of the operating regions of AOIM and A-SOFT. No previous study has been found to discuss this type of hybrid rocket before, but this type should have both the advantages of A-SOFT and AOIM. For example, under the assumption that there is no reverse flow from the aft-chamber to the main chamber, the oxidizer injected into the aft-chamber does not affect fuel regression rates. This characteristic enables the engine to achieve both high regression rates and a simple feedback thrust control. Moreover, applying counter vortex injection to the head-end tangential injection for the aft-chamber injection may enhance mixing of the burnt gas and the oxidizer, enabling to shorten the aft-chamber length.

Providing that the oxidizer injected from the aft-chamber does not affect fuel regression, the operating region of fuel mass flow rates with a given single port grain and total oxidizer mass flow rate is expressed as

$$0 \leq \dot{m}_f \leq 2\pi^{1-n} L_f r_i^{1-2n} \rho_f a \left(1+S_g^2\right)^m {\dot{m}_o}^n \quad (16).$$

The throttle range with a fixed fuel port radius at a constant O/F is evaluated as

$$0 \leq \dot{m}_o \leq \left(2\pi^{1-n} L_f r_i^{1-2n} \rho_f a O/F\right)^{\frac{1}{1-n}} \left(1+S_g^2\right)^{\frac{m}{1-n}} \quad (17).$$

Equations (16) and (17) are equivalent to the region encompassing Eqs. (3) and (10) and that doing Eqs. (4) and (11), respectively. These results also show that Swirling-AOIM has the possibility to cover both the operating regions of AOIM and A-SOFT. Therefore, the throttle range at a constant O/F over a burn is

$$0 \leq \dot{m}_o \leq \left(2\pi^{1-n} L_f r_o^{1-2n} \rho_f a O/F\right)^{\frac{1}{1-n}} \left(1+S_g^2\right)^{\frac{m}{1-n}} \quad (18).$$

For $\left(m, n, S_g\right) = (0.0987[-], 0.651[-], 20[-])$, this equation results that Swirling-AOIM has 5.4 times larger upper throttle limit than AOIM using axial injection.

However, we should note that this method is just a conceptual idea, and this has not been tested. If there is a reverse flow typically observed near the head-end of the fuel port due to a strong tangential injection (Motoe and Shimada, 2014) between the main chamber and aft-chamber, the reverse flow should make it difficult to predict regression rates or achieve feedback thrust control at a constant O/F ratio. Therefore, this injection type should be experimentally tested in the future.

[DOI: 10.1299/xxx.2017xxx000x]

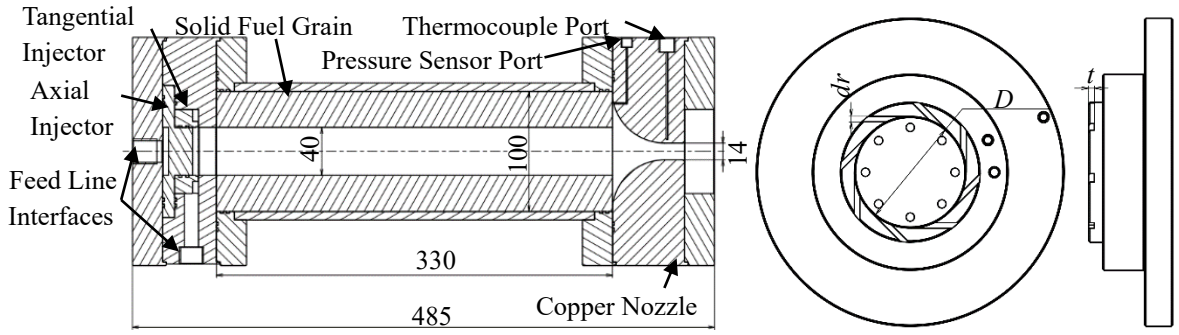

Fig. 3 Typical design of A-SOFT and a dual injector consisting of axial and tangential injectors.

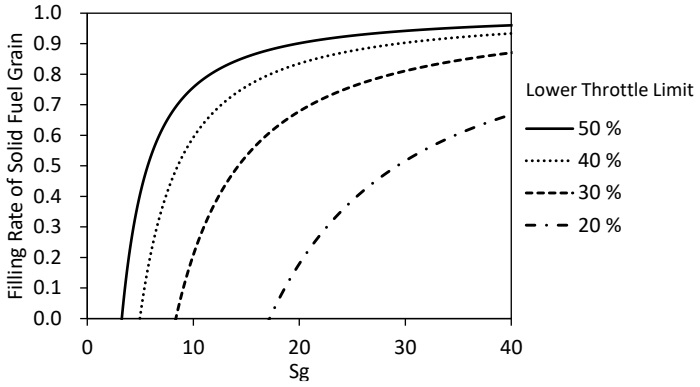

Fig. 4 Packing density of a fuel grain to satisfy the requirement to maintain a specific throttle range for various S_g.

3. Penalties on O/F control systems

Adapting O/F control systems into a hybrid rocket propulsion can affect requirements for the other subsystems in the rocket. These requirements from the engine can increase the structural mass of the other subsystems or the complexity of the whole propulsion system. Therefore, these penalties in the other subsystems of each type should also be taken into account when flight performance is compared among these types of O/F controlled hybrid rockets and the conventional ones. This section discusses these factors for each component affected by the O/F control systems.

3.1 Structural penalty on feed systems

O/F control systems in hybrid rocket propulsion typically require for the oxidizer feed line to split into two branches to control the contribution of the oxidizer flow to the fuel regression. Therefore, O/F controlled hybrid rockets include at least two branches of the oxidizer pipelines and the valves in each branch for the mass flow control, leading to the increase in the mass and complexity of the oxidizer feed systems. Moreover, a complicated feedback control system for the thrust and O/F control can increase the mass of the control circuit and its wiring. In the typical method for the preliminary design analyses of liquid rocket propulsion (Humble, et al., 1995), the mass of these subsystems is included into the 10% structural margin of the major structure in the propulsion system. For simplicity, in this preliminary process, it is reasonable to increase the coefficient of the structural margin by a few percent as the penalty mass for the additional piping, valve, and control electric hardware of the feedback control system.

3.2 Structural penalty on aft-chamber

For AOIM and Swirling-AOIM, mixing of the oxidizer injected from the aft-chamber with the burnt gas requires a longer aft-chamber, resulting in the increase in the structural mass of the aft-chamber and the aspect ratio of the motor. In the typical preliminary design analysis, L/D of aft-chamber for the conventional hybrids vary between 0.5 and 1.0

[DOI: 10.1299/xxx.2017xxx000x]

(Altman and Humble, 1995). The main chambers of AOIM and Swirling-AOIM can also be regarded as fuel-rich gas generators of liquid rocket propulsion. This aspect enables us to see the aft-chamber as the main chamber of a liquid rocket and determine the length of the aft-chamber referring to the design criteria of the combustion chamber based on L* for the liquid rocket using hydrocarbon as the fuel. The reference (Huzel and Huang, 1992) says that L* of liquid rocket propulsion using RP-1 and liquid oxygen and that using RP-1 and hydrogen peroxide range 0.83-1.02 [m] and 1.52-1.78 [m], respectively. For Swirling-AOIM, the counter-vortex injection of the oxidizer can enhance the mixing of the oxidizer with the burnt gas, which may allow shortening the length of the aft-chamber.

3.3 Oxidizer vaporization systems for tangential oxidizer injection

The previous research by Kitagawa and Yuasa (2006) has reported that applying liquid oxidizer to swirling oxidizer injection in hybrid rocket propulsion critically decreases the enhancement of regression rates and causes unstable combustion. This result suggests that A-SOFT and Swirling-AOIM require the tangential oxidizer injection in the gaseous phase and any oxidizer vaporizing system for their feed systems if the oxidizer is stored in the liquid phase. Two candidates of the oxidizer vaporizing system have already been proposed: oxidizer gas generator using hybrid combustion (Mishima, et al., 2016) and regenerative cooling nozzle using liquid oxidizer (Kitagawa et al., 2007). The concepts of these two subsystems have already been demonstrated.

The advantage of the gas generator is its simple structure, but it requires a separate fuel and igniting system only for the gas generator. In order to avoid the complexity of the gas generator using liquid fuel and the uncontrollability of that using solid propellant, Mishima, et al. (2016) proposed an oxidizer gas generator using hybrid combustion. However, it is not easy to practically adopt this idea because the temperature of the oxidizer depends on the surface area of the solid fuel and the oxidizer mass flow rate.

Regenerative cooling nozzles using oxidizer have a large potential to improve the performance of hybrid rocket propulsion because this technology enables to prevent nozzle throat erosion. Liquid oxygen seems to be optimal for this technology because of its low liquid state temperature, but the researching and developing costs tend to be large for the cryogenic feed system and the regenerative cooling nozzle. In addition, the requirement of a long-time burn to confirm the thermal equilibrium of the whole system also increases the building costs of the test facility. The pressure drop in the regenerative cooling nozzle can also be a disadvantage of this solution because the larger feed pressure requires a stronger structure of the feed line in the upstream of the nozzle. One of the major risk factors in the regenerative cooling nozzle is the feasibility of heat exchange to satisfy both the design criteria of the nozzle wall temperature and the requirement for the oxidizer vaporization over the throttle range. The other prominent risk factor is the oxidization of the channel, leading to a decrease in the heat transfer coefficient between the oxidizer and the channel wall. These risk factors may restrict the options of the materials to be used for the regenerative cooling nozzle compared to those used in liquid rocket propulsion.

3.4 Pressure drop in tangential oxidizer injection

The geometry of the tangential injector for A-SOFT and Swirling-AOIM is subject to Eq. (7) for a given S_g whereas the axial injector does not have any explicit condition except its cross-sectional area. This requirement for the S_g practically provides a restriction of the cross-sectional area of the tangential injector. This condition results in a constraint to the supremum of geometric swirl number from the oxidizer mass flow rate from the injector, the total pressure just in the upstream of the injector p_{0_i} [Pa], and the chamber pressure p_c [Pa].

Provided with a fixed $\xi[-] = dr/D$, S_g is written only by the tangential injector area A_i [m^2], the cross-sectional area of the pre-chamber A_{pc} [m^2], and ξ:

$$S_g = \frac{4}{\pi}\frac{A_{pc}(1-\xi)}{A_i} \tag{19}$$

where ξ can be expressed with an area ratio A_i/A_{pc} and injector aspect ratio $\beta = dr/t$ [-] as

$$\xi = \sqrt{\frac{\pi}{4}\frac{\beta A_i}{n_p A_{pc}}} \tag{20}.$$

[DOI: 10.1299/xxx.2017xxx000x]

Different cross-sectional geometries of the tangential injector such as circular cross-section also provide similar relations to Eq. (19). The relation Eq. (19) gives the supremum of S_g with a fixed A_i:

$$\sup(S_g) = \lim_{\beta\to 0}\left(\frac{4}{\pi}\frac{A_{pc}(1-\xi)}{A_i}\right) = \frac{4}{\pi}\frac{A_{pc}}{A_i} \tag{21}$$

Let us assume a combustion at the chemical equilibrium in the main chamber with a given fuel port oxidizer mass flux G_{o_p} [kg/m^{2}s] and O/F under the choking condition at the nozzle throat. The choking condition with a fuel port-nozzle throat aspect ratio χ [-] provides the main chamber pressure p_c:

$$G_t = \chi\left(1+\frac{1}{O/F}\right)G_{o_p} = \frac{p_c}{a_c}\gamma_c\sqrt{\left(\frac{2}{\gamma_c+1}\right)^{\frac{\gamma_c+1}{\gamma_c-1}}} \tag{22}$$

where G_t [kg/m^{2}s], γ_c [-], and a_c [m/s] refer to mass flux at the throat and specific heat ratio and sonic velocity at the main chamber given by the chemical equilibrium when a frozen flow between the main chamber and the nozzle throat is assumed. The area ratio A_i/A_{pc} is evaluated with the mass conservation of the oxidizer. Density and sonic velocity of the oxidizer at the exit of the injector ρ_{o_e} [kg/m^3] and a_{i_e} [m/s] enable us to express the oxidizer mass flow rate at the injector:

$$\dot{m}_o = \rho_{o_c}a_{i_e}M_{i_e}A_i = \gamma_o\frac{p_c}{a_{i_e}}M_{i_e}A_i \tag{23}$$

where γ_o [-] and M_{i_e} [-] refer to the specific heat ratio of the oxidizer and Mach number of the oxidizer at the injector exit, respectively. In the combustion chamber and the nozzle throat, the mass conservation of the oxidizer also gives the following equation:

$$\dot{m}_o = A_pG_{o_p} \tag{24}$$

where A_p [m^2] refers to the cross-sectional area of the fuel port. Under the assumption of $A_p = A_{pc}$, Eqs. (23) and (24) give

$$\frac{A_p}{A_i} = \gamma_o\frac{p_c}{a_{i_e}}\frac{M_{i_e}}{G_{o_p}} \tag{25}$$

The perfect gas assumption gives the following relation between M_{i_e} and the given pressure ratio ϕ $[-] = p_{0_i}/p_c$,

$$M_{i_e} = \sqrt{\frac{2}{\gamma_o-1}\left(\phi^{\frac{\gamma_o-1}{\gamma_o}}-1\right)} \tag{26}$$

where p_{0_i} [Pa] refers to stagnation pressure of the oxidizer. This relation and the isentropic assumption at the injector provide the injector-port area ratio:

$$\frac{A_p}{A_i} = \frac{p_c}{G_{o_p}}\frac{\phi^{\frac{\gamma_o-1}{2\gamma_o}}}{\sqrt{R_oT_{0_i}}}\sqrt{\frac{2\gamma_o}{\gamma_o-1}\left(\phi^{\frac{\gamma_o-1}{\gamma_o}}-1\right)} = \chi\left(1+\frac{1}{O/F}\right)\frac{a_c}{\sqrt{R_oT_{0_i}}}\frac{1}{\gamma_c}\sqrt{\frac{2\gamma_o}{\gamma_o-1}\phi^{\frac{\gamma_o-1}{\gamma_o}}\left(\phi^{\frac{\gamma_o-1}{\gamma_o}}-1\right)\left(\frac{\gamma_c+1}{2}\right)^{\frac{\gamma_c+1}{\gamma_c-1}}} \tag{27}$$

where R_o [J/(kgK)] and T_{0_i} [K] refer to the gas constant of the oxidizer and the stagnation point temperature at the entrance of the injector, respectively. The fuel port aspect ratio AR_{port} [-] corresponding to the given O/F is expressed by

$$AR_{port} = \frac{G_{o_p}^{1-n}}{4\rho_f a\left(1+S_g^2\right)^m O/F} \tag{28}$$

where ρ_f [kg/m^3] refers to the density of the solid fuel. The set of Eqs. (19), (22), (27) and (28) provides S_g, p_c, and AR_{port}, for the given O/F, ϕ, χ, and propellant option regardless of the engine scale.

When the pressure drop includes that of the contraction loss Δp [Pa] between the feed line and the injector, Δp is

[DOI: 10.1299/xxx.2017xxx000x]

approximated by the following fitting model of the characteristics of contraction loss (The Japan Society of Mechanical Engineers ed., 2006) as

$$\phi_{cont} = \frac{\Delta p}{p_c} \sim \begin{cases} 0.4703\left(1 - A_i/A_{feed}\right)\frac{\gamma_o M_{feed}^2}{2}\phi & \left(A_i/A_{feed} \le 1\right) \\ 0 & \left(A_i/A_{feed} > 1\right) \end{cases} \tag{29}$$

where A_{feed} [m^2] is the cross-sectional area of the feed line. The injector-feed line area ratio A_i/A_{feed} is evaluated with the following equation based on the one-dimensional isentropic flow equation:

$$\frac{A_i}{A_{feed}} = \frac{M_{feed}}{M_{i_e}}\left[\frac{(\gamma_o-1)M_{i_e}^2+2}{(\gamma_o-1)M_{feed}^2+2}\right]^{\frac{\gamma_o+1}{2(\gamma_o-1)}} \tag{30}$$

where Mach number in the feed line M_{feed} [-] is assumed to be less than 0.3 as recommended by NASA SP-125 (Gordon and McBride, 1994). Stagnation pressure at the end of the feed line $p_{0_{feed}}$ [Pa] is evaluated by

$$\phi_{feed} = p_{0_{feed}}/p_c = \left(p_{0_i} + \Delta p\right)/p_c = (\phi + \phi_{cont}) \tag{31}.$$

This pressure drop depends on the combination of the fuel and the oxidizer.

The relations among the pressure drop, the available geometric swirl number, and the fuel port aspect ratio were investigated for paraffin and gaseous oxygen (GOX) and paraffin and 90% hydrogen peroxide (90% HP). The pressure drop was evaluated for G_{o_p} = 500, 600, and 700 [kg/m^{2}s] because the lower limit of the blowing-off of the flame in hybrid rocket engines is said to be larger than 700 [kg/ m^{2}s] (Altman and Humble, 1995). The O/Fs for the first propellant option and the latter two options were assumed to be 2 and 7, respectively. For simplicity, these evaluations ignored the increase in local pressure at the wall due to centrifugal pressure induced by the swirling flows in the engine.

3.4.1 Paraffin and GOX

For paraffin and GOX, the GOX at the nozzle exit was assumed to enter at the temperature of 300[K]. Figure (5) a) shows the result of port aspect ratio, pressure drop normalized by p_c, and geometric swirl number when $(\beta, \chi) = (0,\ 2)$ and $(\beta, \chi) = (1,\ 2)$, respectively. It is clear that pressure ratio has a trade-off with the geometric swirl number and port aspect ratio. $\beta = 0$ provides the supremum of geometric swirl number. χ larger than 2 is required to stabilize the flame, and that larger than 3 is recommended in chemical rocket propulsion systems, though a small χ is favorable from the aspect of the packing density of the solid fuel grain. The right and left ends of the curves show the results under the choking condition of the tangential injector and those with a 1% pressure drop ϕ in the choking condition.

When $G_{o_p} = 700$ [kg/m^{2}s], $\beta = 0$ and $\chi = 2$, the tangential injection theoretically had a potential to provide $\sup(S_g)$ of 32.7 under the choking condition with a slight sensitivity to G_{o_p}, because the term of T_c and γ_c in Eq. (27) has a less sensitivity in this range of G_{o_p}. However, such a large geometric swirl number required a large pressure ratio of 2.07. In contrast, even with a small pressure ratio ϕ_{feed} of 1.01, the tangential injector with $\sup(S_g) = 3.4$ gave AR_{port} of 12.5 compared to AR_{port} of 16.0 in axial injection. The curve of pressure ratio ϕ_{feed} was hardly affected by G_{o_p} because the effect of G_{o_p} on the term of T_c and γ_c appearing in Eq. (27) was negligible. This curve had a cusp at $\sup(S_g)$ =9.2, at which the injector port exit area is equal to that of the feed line. The port aspect ratio AR_{port} had an obvious sensitivity to G_{o_p}, which is shown as $G_{o_p}^{1-n}$ in Eq. (28). ϕ_{cont} increased with increasing S_g but had less than 9.2% of ϕ over all the cases.

$\beta = 1$ corresponds to a tangential injector with square ports. AR_{port} when $\beta = 1$ was plotted on the same curve when $\beta = 0$, for each G_{o_p}, because β did not influence the relation between S_g and AR_{port} as shown in Eq. (28). The left and right ends of all the curves when $\beta = 1$ shifted to S_g = 2.7 and 31, respectively. The pressure ratio ϕ_{feed} when $\beta = 1$ was also common, regardless of G_{o_p}, and it had the same range as that when $\beta = 0$. The cusp of the curve was located at $S_g = 8.1$ and had the same ϕ_{feed} of that when $\beta = 0$. It was unexpected but clarified that such an un-optimized injector has similar characteristics of S_g and AR_{port} to those of the upper limit of S_g.

Figure (5) b) shows the relations among ϕ_{feed}, AR_{port}, and S_g when $\chi = 3$. The decrease in p_c due to the larger throat area allowed to broaden the range of S_g up to 49 when $\beta = 0$ and 47 when $\beta = 1$, respectively. However, all the curves had similar trends to those when $\chi = 2$. ϕ_{feed} had the same range as that when $\chi = 2$, from 1.01 and 2.07. The left and right ends of the curve of AR_{port} when $\beta = 1$ and $G_{o_p} = 700$ [kg/m^{2}s] were 12.0 and 7.51, respectively.

[DOI: 10.1299/xxx.2017xxx000x]

This shift to the smaller aspect ratios was due to the larger surface area of the fuel port.

These results say that the tangential injection with a large swirl number enables to decrease AR_{port}, but 50% higher feed pressure should be taken into account to feed the GOX with a large S_g larger than 30. This pressure drop will strongly impact on the structure of the feed system, especially when a gas pressure feed system is adopted.

3.4.2 Paraffin and 90% HP

The previous study (Karabeyoglu, et al., 2014) has pointed out that propellants with large optimal O/Fs such as hydrocarbon and HP, by nature have a less sensitivity of specific impulse to O/F shifts. However, mass penalties for residual propellants may have a relatively larger impact on flight performance than those for propellants with a small optimal O/F because a 10% larger regression rate than expected causes a residual oxidizer corresponding to 6.1% of the sum of the fuel and the oxidizer when O/F=2 but to a 8.0% when O/F=7. Therefore, there can also be a significance to adopt O/F control technologies for hybrids with a large optimal O/F.

For paraffin and 90% HP, the oxidizer is assumed to be decomposed with a catalyst in the upstream of the injector under an adiabatic condition. The temperature of 90% HP is assumed to be 300 [K] before the decomposition, and the decomposed gas is assumed as a frozen flow with a mass fraction at the pressure of p_c. The regression rate behavior was modeled as $(a, m, n) = (1.08 \times 10^{-4}, 1.67, 0.965)$ for Eq. (6) referring to the previous studies on paraffin and HP (Brown and Lydon, 2005). The parameter m to represent the sensitivity to effective geometric swirl number was assumed to be the same as the estimated value of m for high density polyethylene (HDPE) and 87.5% HP (Messineo, et al., 2016). For this estimation, the regression rate coefficient of n of 0.75 was used from the previous experimental data of axial hybrids with HDPE and 90% HP (Wernimont and Heister, 1996).

Figure (5) c) and d) show the relations among ϕ_{feed}, AR_{port}, and S_g for all the calculated cases on paraffin and 90% HP. The large O/F does not require a large mass flow rate of fuel regression, leading to quite small AR_{port} in the range from 4×10^{-4} to 1.1. The large O/F and the large temperature of the decomposed oxidizer increased A_i to supply the large mass flow rates of the oxidizer with the same range of ϕ, leading to the decrease in the range of S_g and $\sup(S_g)$. The sensitivities to χ, G_{o_p} or β were hardly observed on the curves of AR_{port} vs S_g. The relation between ϕ_{feed} and S_g had an ignorable sensitivity to G_{o_p} as in the case of paraffin and GOX. The range of ϕ_{feed} hardly shifted in spite of the difference in γ_o from 1.40 for GOX to 1.26 for the decomposed 90% HP. The shapes of these curves with the cusps were quite similar to those in paraffin and GOX.

The result of this analysis suggests that for a propellant with a large optimal O/F, it is difficult to apply a large S_g because the cross-sectional area of the tangential injector tends to become large to supply a large oxidizer mass flow rate. This characteristic makes pressure drop large for the S_g applied and the control range of fuel mass flow rates smaller. In terms of the length of the grain, the large m drastically decreases AR_{port}, which is small even for axial injection, especially in the range of S_g from 0.58 to 4.0. This is because axial injection or small geometric swirl number less than 4 even gives enough regression rates and port aspect ratio for the optimal O/F of wax and HP. This result suggests that AOIM or Swirling-AOIM with a small S_g has a good applicability for wax and HP because A-SOFT with a small S_g cannot provide enough control ranges of O/F.

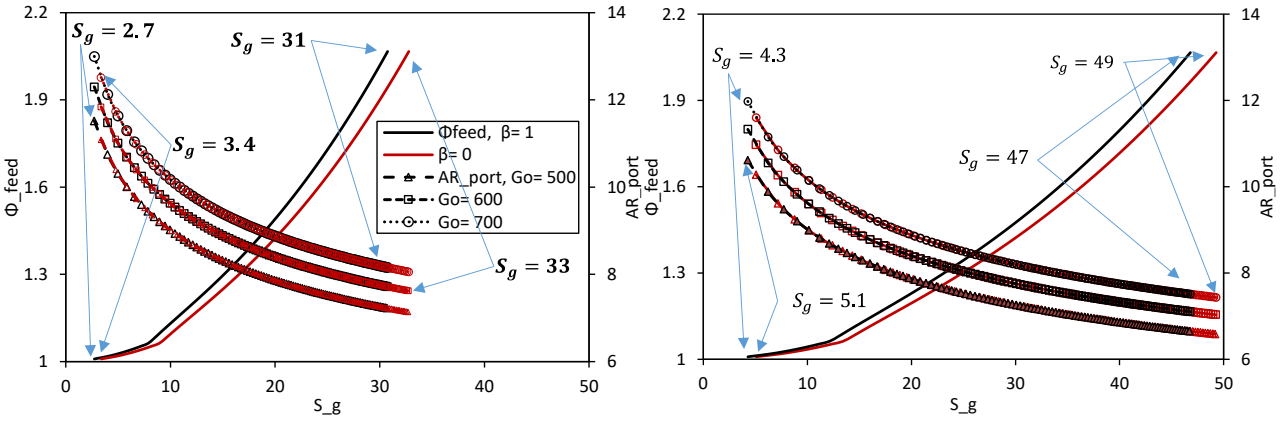

a) $\chi = 2$, paraffin and GOX

b) $\chi = 3$, paraffin and GOX

[DOI: 10.1299/xxx.2017xxx000x]

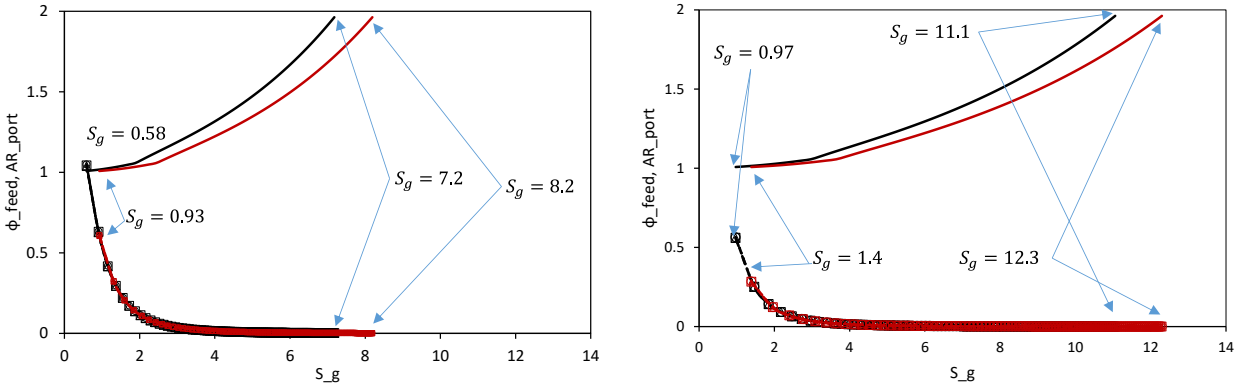

c) $\chi = 2$, paraffin and 90% HP d) $\chi = 3$, paraffin and 90% HP

Fig. 5 Relations between pressure drop ϕ_{feed}, port aspect ratio AR_{port}, and S_g.

4. Applicability of O/F control methods to various scales and propellants

The individual O/F control methods should have their suitable scales of thrust and propellant options. The discussion on this topic usually requires one to solve design problems including their subsystems and structure to bear the maximum load during the flight. However, such evaluations are too complex for this preliminary study. This study only considers the feasibility of the motors with a single fuel port for 1st stage of satellite launchers under the given conditions of aspect ratio, initial acceleration, propellant option, and initial mass of the propellant.

This research evaluates the feasibility of the requirements at the lift-off because rocket propulsion systems are usually required to output their full throttle at the lift-off for the maximum mass of the rocket during the flight in spite of the smallest fuel surface area of the single port grain over the burn. The main evaluation values are the required regression rate and the effective density of the propellant at the lift-off. The feasibility of the required regression rate is compared with the regression rate behavior Eq. (6).

In this problem, the design solutions of the regression rate $\dot{r}$, the outer diameter of the fuel grain r_o, and the inner-outer diameter ratio of the fuel grain ϕ [-] are evaluated for the required acceleration parameter α [m/s^2], the aspect ratio of the motor and tank AR [-], and the mass of the propellant m_p [kg] under the given O/F and the oxidizer mass flux $G_{o_{max}}$ [kg/m^{2}s]. These required parameters are defined as

$$\begin{cases} \alpha(\dot{r}, r_o, \phi) = \frac{\dot{m}_p I_{sp} g}{m_p} \\ AR(\dot{r}, r_o, \phi) = \frac{L_{tot}}{2r_o} \\ m_p(\dot{r}, r_o, \phi) = m_f + m_o \end{cases} \tag{32}$$

where I_{sp} [s], g [m/s^2] refer to the given specific impulse and gravitational acceleration, respectively, L_{tot} [m] refers to the total length of the motor and the oxidizer tank, and the m_f [kg] and m_o [kg] refer to the initial mass of the fuel and oxidizer, respectively. These parameters are expressed as functions of the three design variables independent of each other.

The geometry of the fuel grain port provides us with an expression of acceleration parameter in the design variables as

$$\alpha(\dot{r}, r_o, \phi) = \frac{\dot{m}_f}{m_f} I_{sp} g = 2 \frac{\dot{r}}{r_o} \frac{\phi}{1-\phi^2} I_{sp} g \tag{33}.$$

The length of the propulsion system L_{tot} [m] seen in $AR(\dot{r}, r_o, \phi)$ is evaluated under the assumption that the O/F of the propellant is equal to that of the propellant mass flow at the lift-off. This assumption is expressed by the following equation:

$$\frac{O}{F} = \frac{\phi r_o G_{o_{max}}}{2\rho_f \dot{r} L_f} = \frac{\rho_{o_s} L_o}{\rho_f (1-\phi^2) L_f} \tag{34}$$

where L_f [m], L_o [m], and ρ_{o_s} [kg/m^3] refer to the lengths of the fuel grain and the oxidizer tank and the density of the stored oxidizer. This assumption gives the expressions of L_f, L_o in the independent design variables as

[DOI: 10.1299/xxx.2017xxx000x]

$$\begin{cases} \rho_{o_s} L_o = \frac{\phi r_o G_{o_{max}} (1-\phi^2)}{2\dot{r}} \\ \rho_f L_f = \frac{\phi r_o G_{o_{max}}}{2\dot{r} O/F} \end{cases} \quad (35).$$

Combining Eqs. (32) and (35) provides the expression of AR as a function of $\dot{r}, r_o$ and ϕ:

$$AR(\dot{r}, r_o, \phi) = \frac{L_o + L_f + L_{aft}}{2r_o} = \frac{G_{o_{max}} \phi (1-\phi^2)}{4\rho_{o_s} \dot{r}} + \frac{G_{o_{max}} \phi}{2O/F \rho_f \dot{r}} + \lambda \quad (36)$$

where L_{aft} [m] refers to the length of the aft-chamber and λ [-] is defined as $\lambda \equiv L_{aft}/2r_o$. According to the reference (Altman and Humble, 1995), λ for conventional hybrids is designed between 0.5 and 1.0. This research gives the following constants to λ for each O/F control method.

$$\lambda = \begin{cases} 0.5 & \cdots \quad (A-SOFT) \\ 1.0 & \cdots \quad (AOIM, S-AOIM) \end{cases} \quad (37).$$

The initial mass of the propellants m_p is also expressed with the independent design variables using Eq. (35):

$$m_p = \left(1 + \frac{1}{O/F}\right) m_o = \pi \left(1 + \frac{1}{O/F}\right) \rho_{o_s} L_o r_o^2 = \frac{\pi}{2} \left(1 + \frac{1}{O/F}\right) r_o^3 \frac{G_{o_{max}} \phi (1-\phi^2)}{\dot{r}} \quad (38).$$

The set of Eqs. (33), (36) and (38) should be solved for the target α, AR, and m_p. These three equations are summarized into the following single equation of ϕ:

$$\phi^5 - \left(1 + \frac{2\rho_{o_s}}{\rho_f O/F}\right) \phi^3 - 2(AR - \lambda) \rho_{o_s} \sqrt{\left(\frac{\alpha}{G_{o_{max}} I_{sp} g}\right)^3 \frac{m_p O/F}{\pi(1+O/F)}}\, \phi^2 + 2(AR - \lambda) \rho_{o_s} \sqrt{\left(\frac{\alpha}{G_{o_{max}} I_{sp} g}\right)^3 \frac{m_p O/F}{\pi(1+O/F)}} = 0 \quad (39).$$

This equation is numerically solved to evaluate the packing density and feasibility of the regression rate for each O/F control method.

The required regression rate and the outer diameter are calculated from the solution of ϕ and compared between the propellant options of paraffin and liquid oxygen (LOX) and paraffin and 90% HP. The effective density ρ_e [kg/m^3] is defined as

$$\rho_e = \frac{m_p}{2\pi r_o^3 AR} \quad (40).$$

The mass of propellants m_p, aspect ratio AR and acceleration parameter α range between 1 and 1000 [ton], 4 and 12, and 15 and 20 [m/s^2], respectively. These ranges were set referring to the 1st stages of the various scales of satellite launchers as is shown in Table 1. α of SS-520 and L-4S is exceptionally large (larger than 80 [m/s^2]) probably because the first stages of these two types are originally designed for sounding rockets and the associated particular trajectories. Therefore, this research does not calculate the design solutions for α larger than 30 [m/s^2]. The other constant design parameters are summarized in Table 2. All the constant design parameters are the same as in 3.1 and 3.2, but $G_{o_{max}}$ is fixed to 500 [kg/m^{2}s] because it is not clear whether $G_{o_{max}}$ larger than 500 [kg/m^{2}s] is applicable also to large propulsion systems with an initial propellant mass larger than 100 [ton]. λ has the two options of 0.5 and 1.0 for A-SOFT and AOIMs including Swirling-AOIM, respectively.

4.1 Paraffin and LOX

Figure (6) a) and b) summarize the results of ρ_e and required $\dot{r}$ and S_g for A-SOFT with $\alpha =$ 15 and 20 [m/s^2], respectively. The required $\dot{r}$ gradually increases but the corresponding S_g increases drastically with the increasing order of magnitude of m_p. For example, when $AR =$ 8 and $\alpha =$ 15[m/s^2], the required S_g for the m_p of 100 [ton] is about 30 and a large S_g from 30 to 50 can slightly increase m_p. An m_p more than 1000 [ton] does not give a design solution without choking at the injector for this configuration. This trend does not change for a different α and AR though the feasible m_p increases with increasing AR or decreasing α. On the other hand, a large AR sometimes gives

[DOI: 10.1299/xxx.2017xxx000x]

a solution which does not require a positive S_g. When α =15 [m/s^2] and $AR = 12$ [ton], the regression rate with axial injection is larger than that required from the design solution with a m_p less than 8 [ton]. A-SOFT is not applicable for these cases because this type cannot provide a regression rate less than that with axial injection. For an arbitrary AR, ρ_e decreases with increasing m_p. This effect is relatively small for a large AR, and ρ_e in the 100 to 1000 [ton] range of m_p slightly depended on AR. The relation between AR and m_p is reversed when $m_p = 4096$ [ton]. The increase in α affects ρ_e especially in the range of $m_p > 100$ [ton] while this raise the required $\dot{r}$ by about 10%. When $\alpha = 15$ [m/s^2], ρ_e decreased from 550 [kg/m^3] to 475-525 [kg/m^3] in the 300 to 4000 [ton] range of m_p. In contrast, when $\alpha = 20$ [m/s^2], ρ_e decreased from 550 [kg/m^3] to 425-500 [kg/m^3] in the same range of m_p.

Figures (6) c) and d) summarize the results for AOIMs. AOIMs had similar characteristics of the required $\dot{r}$ and ρ_e to those of A-SOFT, but the required $\dot{r}$ for AOIMs were 5-10% larger than that for A-SOFT. It is easy to understand that tangential injection is required when $\alpha = 15$ [m/s^2] and m_p is larger than 8 [ton] for an AR calculated in this evaluation. This result indicates that tangential injection should be adopted for AOIM when the propulsion system is scaled up in a larger m_p than 10 [ton]. When $AR = 10$, $\alpha = 15$ [m/s^2] and $m_p = 128$ [ton], the required $\dot{r}$ of A-SOFT was 9.9 whereas that of AOIMs was 10.3. This increase in the required $\dot{r}$ slightly decreases the upper limit of the scaling-up of the propulsion system. The adoption of AOIM decreased ρ_e by 50 to 100 [kg/m^3] compared to that of A-SOFTs mainly due to the increase in the volume of the aft-chamber. ρ_e for a small AR decreased more than those for large AR in a small m_p.

4.2 Paraffin and 90% HP

Figure (7) a) and b) summarize the results of ρ_e and required $\dot{r}$ and S_g for A-SOFT when $\alpha =$ 15 and 20 [m/s^2], respectively. Both the trends of the required $\dot{r}$ and ρ_e for AR and m_p were quite similar to those for paraffin and LOX. The required $\dot{r}$ was smaller than that of paraffin and LOX because of the high optimal O/F of 7. The required $\dot{r}$ ranged from 4 to 20 [mm/s] over the range of m_p analyzed. 90% HP with larger density than LOX achieved ρ_e more than 800 [kg/m^3] in the 1-100 [ton] range of m_p. The corresponding S_g for the required $\dot{r}$ is positive owing to a large regression rate behavior and the large swirl number exponent m only when $AR = 4$. However, we should note that this regression rate behavior is the result of the extrapolation of the burn tests with lower oxidizer mass flux and the further experiments are required for a larger oxidizer mass flux. The difference in $\dot{r}$ and ρ_e between $\alpha =$ 15 and 20 [m/s^2] were also similar to that of paraffin and LOX. The required $\dot{r}$ for $\alpha = 20$ [m/s^2] increased by 10%, and ρ_e was affected by the increase in α especially for a large m_p. Also for this propellant option, the dependence of ρ_e on AR reverses around a m_p of 1000 [ton]. For $\alpha =$ 20 [m/s^2], $m_p = 4096$ [ton] and $AR = 12$, ρ_e goes down to 497 [kg/m^3].

Figure (7) c) and d) summarize the results of ρ_e and the required $\dot{r}$ and S_g for AOIMs when $\alpha =$ 15 and 20 [m/s^2], respectively. The regression rate with axial injection is large enough even for large-scale rockets larger and a small aspect ratio analyzed in this calculation. Tangential injection is required only when $AR = 4$ and $m_p \geq 64$ [ton]. Also for paraffin and 90% HP, the propulsion systems with small AR are strongly affected by the increase in the volume of the aft-chamber. For example, ρ_e for AOIMs with $AR = 4$ and $m_p = 1$ [ton] was 800 [kg/m^3] whereas that for A-SOFT was more than 900 [kg/m^3], and the required $\dot{r}$ for AOIMs are also 5-15% larger than that for A-SOFT. These trends are also observed in the last subsection.

The analysis has revealed that the regression rate behavior of paraffin and 90% HP is too large for the small-scale propulsion systems when $m_p \leq 100$ [ton], but this large regression rate also means that the paraffin combined with 90% HP has an enough margin to improve the mechanical property of the solid fuel such as strength and ease of casting, which usually has a trade-off relation with the regression rate. Moreover, such a large $\dot{r}$ is rather favorable for the large-scale propulsion systems. For this propellant option, AOIMs are favorable because these types are theoretically controllable right from 0 % regression rate. If the modification of the fuel to improve its mechanical property also succeeded in the moderation of the regression rate, A-SOFT may also become a good candidate of the O/F control method. However, A-SOFT does not have a potential to cover such a wide throttle range from 0% because the lower limit of thrust for A-SOFT is the same as the axial-only injection. Therefore, we can conclude that the best option for wax and 90% HP is AOIM or Swirling-AOIM.

[DOI: 10.1299/xxx.2017xxx000x]

Table 1 Specifications of the 1st stage of the historic rockets. "*" refers to estimation from available data.

Rocket	Propellant Mass [ton]	Thrust [tonf]	α [m/s^2]	Diameter [m]	Length [m]	Aspect Ratio
SS-520 (Matsuno, et al., 1982)	1.50	13.0	85.0	0.52	5.39	10.3
L-4S (Akiba and Matsuo, 1976)	4.90	41.0	82.1	0.74	8.38	11.4
Electron (RocketLab, 2018)	9.25*	16.5	17.5	1.20	12.1*	10.1
Epsilon (JAXA, 2018a), (JAXA, 2018b)	66.0	208	15.6	2.60	11.7	4.50
H-II (Fukushima, 1994), (Sano et al., 1998)	204	402	30.8	4.00	35.0	8.75
Falcon 9 (SpaceX, 2018)	396	776	19.3	3.66*	42.6*	11.6*
Saturn V (Bilstein, 2003)	2077	3365	19.2	10.1	42.0	4.16

Table 2 Summary of the given design parameters for the sizing of the 1st stage for satellite launchers.

Propellant	Type	I_{sp}[s]	O/F	G_o [kg/m^{2}s]	$(a[\mathrm{kg}^{-n}\mathrm{m}^{1+2n}\mathrm{s}^{n-1}], m, n)$	λ	ρ_f [kg/m^3]	ρ_{o_s} [kg/m^3]
Paraffin/LOX	A-SOFT	280	2	500	(1.08×10^{-4}, 0.0987, 0.640)	0.5	760	1140
Paraffin/LOX	AOIMs	280	2	500	(1.08×10^{-4}, 0.0987, 0.640)	1.0	760	1140
Paraffin/90%HP	A-SOFT	260	7	500	(3.44×10^{-5}, 1.67, 0.965)	0.5	760	1450
Paraffin/90%HP	AOIMs	260	7	500	(3.44×10^{-5}, 1.67, 0.965)	1.0	760	1450

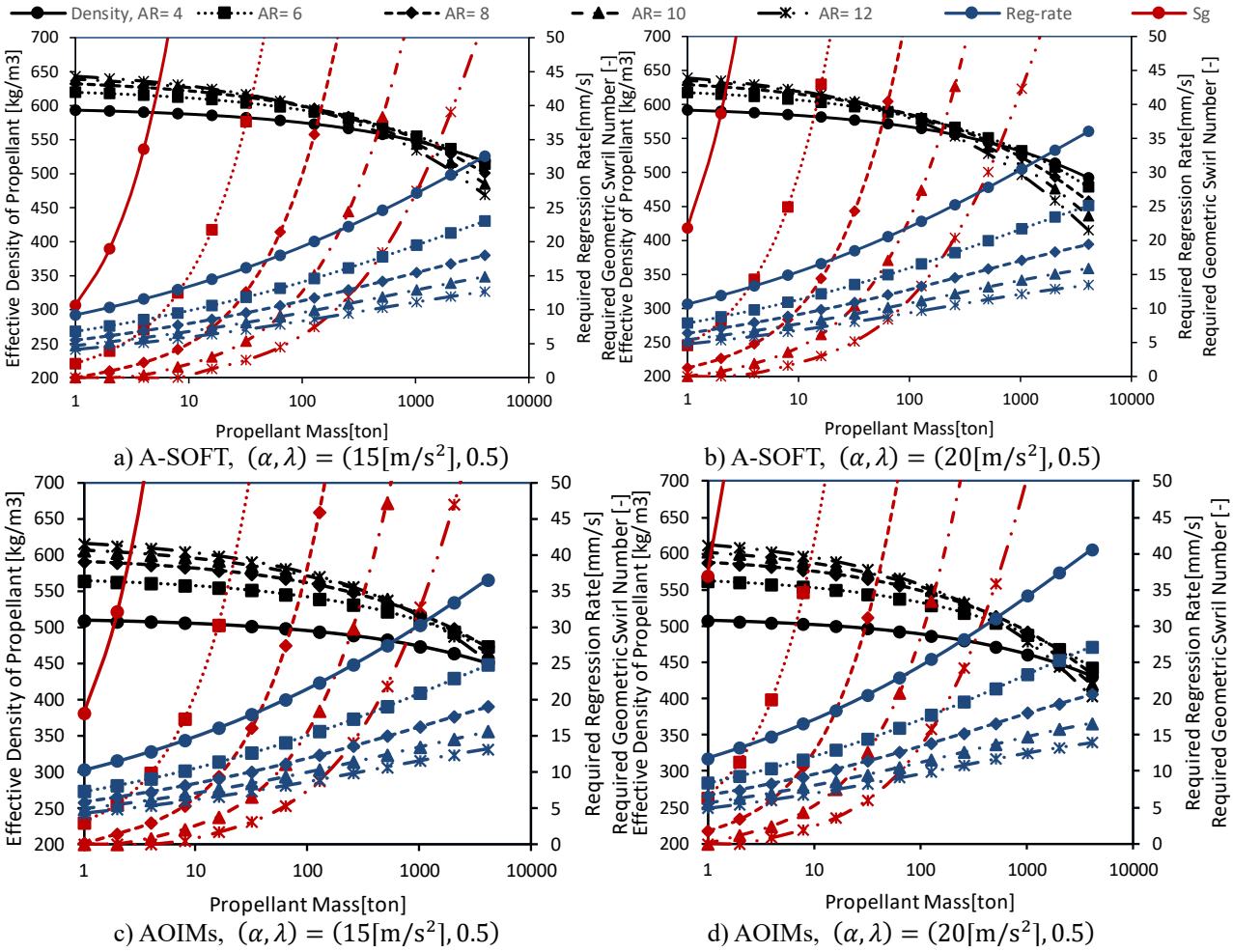

Fig. 6 Summary of the effective density of propellants, the required regression rate, and the corresponding geometric swirl number for various scale and aspect ratio of the 1st stage of the satellite launchers using paraffin and LOX.

[DOI: 10.1299/xxx.2017xxx000x]

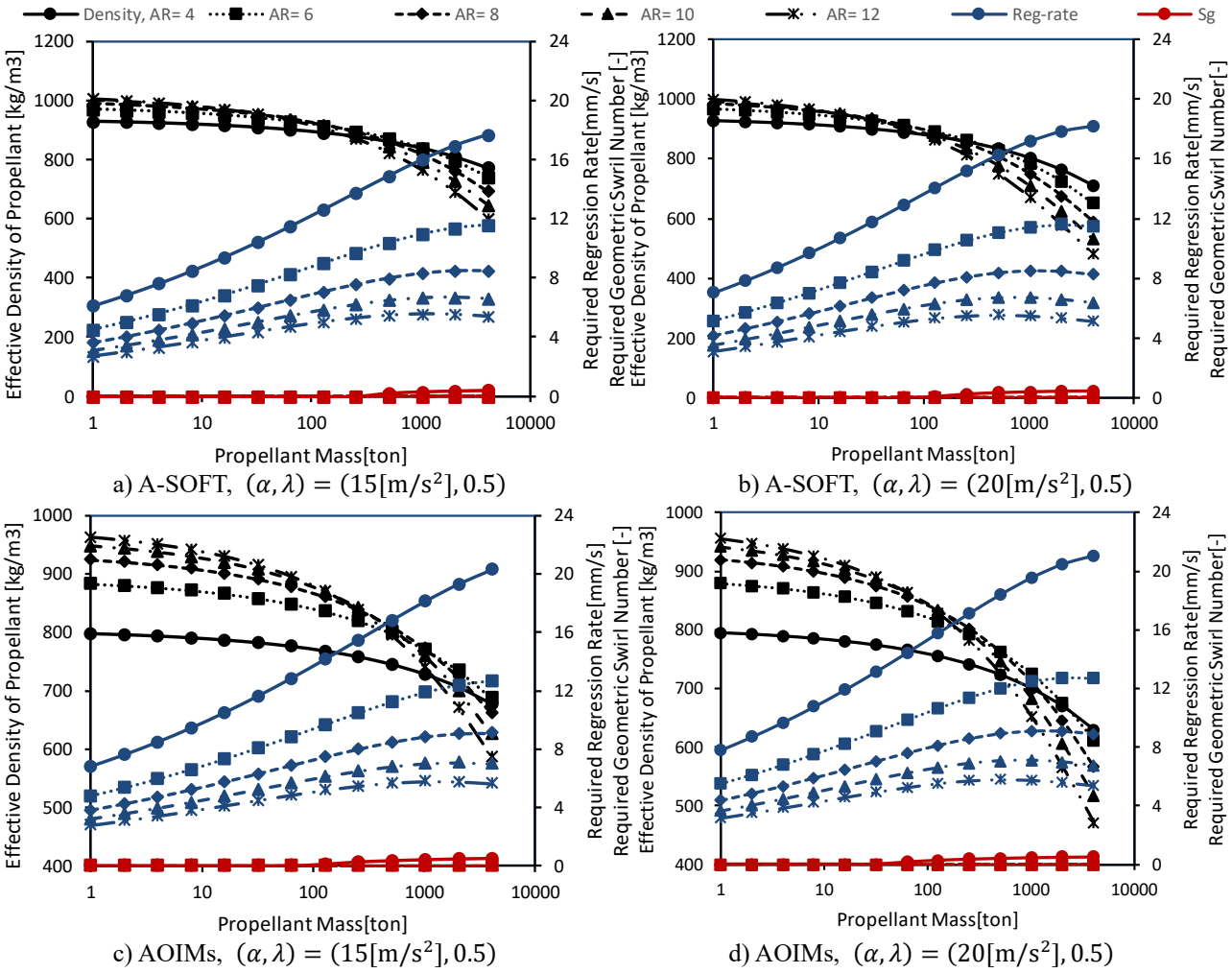

Fig. 7 Summary of the effective density of propellants, the required regression rate and, the corresponding geometric swirl number for various scale and aspect ratio of the 1st stage of the satellite launchers using paraffin and 90% HP.

5. Conclusions

In this research, the three representative O/F control methods for hybrid rocket propulsion, A-SOFT, AOIM, and Swirling-AOIM, were compared to evaluate their characteristics from several aspects.

In Section 2, geometric discussion derived from fuel regression rate behavior revealed that A-SOFT has the upper limit and lower limits of throttle whereas AOIM only has the upper limit. Their two operating regions are theoretically complimentary to each other. This result indicated that Swirling-AOIM has the broadest throttle range. Especially for A-SOFT, the required fuel grain diameter ratio was analytically expressed. This criterion showed that it is possible to design a motor capable of maintaining the 50-100% throttle over a burn using paraffin and GOX.

In Section 3, penalties or disadvantages on the adoption of O/F control methods were discussed. All the methods should increase the complexity and the structure mass of the feed systems compared to conventional hybrids. A-SOFT and Swirling-AOIM require an oxidizer vaporization system to stabilize the combustion and gain the enhancement of the regression rates. The pressure drop for the gaseous oxidizer injection of A-SOFT and Swirling-AOIM has also been modeled in Section 3. The contraction loss between the feed line and the injector with converging nozzles has been evaluated. The upper limit of feed pressure or choking condition gives an upper limit of S_g. The supremum of S_g depends on χ. $\sup(S_g)$ is about 50 for paraffin and GOX and that for paraffin and 90% HP is about 11 when χ is 3. For the choking condition, the stagnation pressure became approximately double of the main-chamber pressure.

In Section 4, a simple design problem has been established to determine the geometries of the fuel and oxidizer tank for O/F-controlled hybrid rockets. The numerical solutions of this problem have revealed that A-SOFT is suitable to a

[DOI: 10.1299/xxx.2017xxx000x]

propulsion system with a propellant mass of 10^0-10^2 [ton], with a middle aspect ratio from 8 to 12 whereas AOIMs are good methods for large-scale motors 10^2-10^4 [ton], with a smaller aspect ratio. For paraffin and LOX, AOIM without tangential injection does not achieve the designed regression rates whereas the other two methods using tangential injection are feasible for achieving the required regression rates. For paraffin and 90% HP, AOIMs are more suitable than A-SOFT because a narrow range of S_g should severely restrict the throttle range. The pair of paraffin and 90% HP has an enough margin of regression rates for those with a propellant mass of 10^0-10^2 [ton] even for axial injection. This large margin will allow improving the mechanical properties of solid fuels, which typically have a trade-off relation with regression rates. Swirling-AOIM has enough regression rates also for the engines with a large propellant mass and a small aspect ratio.

These findings on the three O/F control methods will be applicable to various conceptual design problems of the O/F controlled hybrid rockets. The remaining topics to be considered are the conceptual design and performance analysis integrated with the feed systems, tank design, and motor case design, finally leading to the flight simulations for satellite launchers.

Acknowledgements

This research was supported by the Hybrid Rocket Research Working Group (HRrWG) of the Institute of Space and Astronautical Science, Japan Aerospace Exploration Agency. The authors thank members of HRrWG for their helpful discussion.

This work was also financially supported by JSPS KAKENHI 15J08028.

References

Akiba, R. and Matsuo, H., Progress of the Development of Sounding Rockets for Scientific Measurement: 2. System Design and Development of Motor (Part 2), Journal of the Japan Society for Aeronautical and Space Sciences (1976), Vol. 24, No.267, pp. 169-180 (in Japanese).

Altman, D. and Humble, R., Hybrid Rocket Propulsion Systems, Space Propulsion Analysis and Design (1995), edited by Humble, R. W., Henry, N. G., Larson, and W., J., pp. 365-441, McGraw-Hill.

Bilstein, R., Stages to Saturn: A Technological History of the Apollo/Saturn Launch Vehicles (2003), University Press of Florida.

Boardman, T., Porter, L., Brasfield, F. and Abel, T., An Ultrasonic Fuel Regression Rate Measurement Technique for Mixture Ratio Control of a Hybrid Motor, 31st AIAA/SAE/ASME/ASEE Joint Propulsion Conference and Exhibit (1995), AlAA 95-3081.

Brown, T., R. and Lydon, M., C., Testing of Paraffin-Based Hybrid Rocket Fuel Using Hydrogen Peroxide Oxidizer, Colorado Undergraduate Space Research Symposium Proceedings, University of Colorado Boulder (2005).

Fukushima, Y., Development of H-II Rocket, Proceedings of HOPE/OREX Workshop, Special Issue of National Aerospace Laboratory of Japan (1994), Vol. 24 (in Japanese).

Gordon, S. and McBride, J. B., Computer Program for Calculation of Complex Chemical Equilibrium Compositions and Applications, NASA Reference Publication 1311 (1994), NASA.

Humble, R. W., Lewis, D., Bissell, W. and Sackheim, R., Liquid Rocket Propulsion Systems, Space Propulsion Analysis and Design (1995), edited by Humble, R. W., Henry, N. G., and Larson, W., J., pp. 179-294, McGraw-Hill.

Huzel, D., K. and Huang, D., H., Modern Engineering for Design of Liquid-Propellant Rocket Engines (1992), pp. 71-72, AIAA.

Japan Aerospace Exploration Agency, FY H29 Planning of Rocket Launch: ASNARO-2 and Epsilon 3 (in Japanese), (online), Japan Aerospace Exploration Agency, available from <http://www.jaxa.jp/press/2017/12/20171208_epsilon3_j.html>, (accessed on 28 February, 2018a).

Japan Aerospace Exploration Agency, Result of the Static Firing Test of the Improved Version of SRB-A for H-IIA (in Japanese), (online), Japan Aerospace Exploration Agency, available from <http://www.jaxa.jp/press/2005/01/20050112_srb-a_j.html>, (accessed on 28 February, 2018b).

Karabeyoglu, M., Toson, E. and Evans, B., “O/F Shift” in Hybrid Rockets, 50th AIAA/ASME/SAE/ASEE Joint Propulsion Conference (2014), AIAA 2014-3851.

[DOI: 10.1299/xxx.2017xxx000x]

Kitagawa, K and Yuasa, S., Combustion Characteristics of a Swirling LOX Type Hybrid Rocket Engine, Journal of the Japan Society for Aeronautical and Space Sciences (2006), Vol. 54, No.629, pp. 242-249 (in Japanese).

Kitagawa, K., Sakurazawa, T. and Yuasa, S., Combustion Experiment to Evaluate a LOX Vaporization Nozzle for a Swirling-Oxidizer-Flow-Type Hybrid Rocket Engine with a 1500N-Thrust, Space Technology (2007), Vol. 6, pp. 47-54 (in Japanese).

Marxman, G. A., Wooldridge, C. E., and Muzzy, R. J., Fundamentals of Hybrid Boundary Layer Combustion, Heterogeneous Combustion Conference (1963), AIAA 63-505.

Matsuno, H., Kohno, M., Onoda, J., Kawashima, T., Murakami, T., and Onojima, N., Development of the S-520 Single Stage Sounding Rocket, Acta Astronautica (1982), Vol. 9, No. 10, pp. 631–635.

Messineom, J., Lestrade, J.-Y., Hijlkema, J., and Anthoine, J., 3D Miles Simulation of a Hybrid Rocket with SWIRL Injection, Space Propulsion 2016 (2016), SP2016_3125046.

Mishima, G., Kitagawa, K. and Shimada, T., Feasibility Study of Pre-Burner Lox Vaporization for Swirl Injection Hybrid Rocket Engine, Asian Joint Conference on Propulsion and Power 2016 (2016), AJCPP2016-095.

Motoe, M. and Shimada, T., Numerical Simulations of Combustive Flows in a Swirling-Oxidizer-Flow-Type Hybrid Rocket, 52nd Aerospace Sciences Meeting (2014), AIAA 2014-0310.

Ozawa K., Usuki T., Mishima G., Kitagawa K., Yamashita M., Mizuchi M., Aso S., Tani Y., Wada Y. and Shimada T., Static Burning Tests on a Bread Board Model of Altering-intensity Swirling-Oxidizer-Flow-Type Hybrid Rocket Engine, 52nd AIAA/SAE/ASEE Joint Propulsion Conference (2016), AIAA 2016-4964.

Ozawa, K. and Shimada, T., Effects of O/F Shifts on Flight Performances of Vertically Launched Hybrid Sounding Rockets, 53rd AIAA/SAE/ASEE Joint Propulsion Conference (2017), AIAA 2017-5051.

Ozawa, K. and Shimada, T., Flight Performance Simulations of Vertical Launched Sounding Rockets Using Altering-Intensity Swirling-Oxidizer-Flow-Type Hybrid Motors, 51st AIAA/SAE/ASEE Joint Propulsion Conference (2015), AIAA 2015-3832.

RocketLab, Electron, available from < https://rocketlabusa.com/electron/ >, RocketLab, (accessed on 28 February, 2018).

Sano, N., Kiuchi, S. and Yamada, T., Solid Rocket Booster of H-IIA Rocket, Journal of the Japan Society for Aeronautical and Space Sciences (1997), Vol. 46, No. 535, pp. 449-452 (in Japanese).

Shimada, T., Yuasa, S., Nagata, H., Aso, S., Nak agawa, I., Sawada, K., Hori, K., Kanazaki, M., Chiba, K., Sakurai, T., Morita, T., Kitagawa, K., Wada, Y., Nakata, D., Motoe, M., Funami,Y., Ozawa, K., Usuki, T., Hybrid Propulsion Technology Development in Japan for Economic Space Launch, Chemical Rocket Propulsion: A Comprehensive Survey of Energetic Materials, edited by L., De Luca, T., Shimada, V., P., Sinditskii, and M. Calabro, (2017), Springer Aerospace Technology, Cham, pp. 545-575, Springer International Publishing.

SpaceX, Falcon 9, (online), SpaceX, available from < http://www.spacex.com/falcon9 >, (accessed on 28 February, 2018).

Tamura, T., Yuasa, S. and Yamamoto, K., Effects of Swirling Oxidizer Flow on Fuel Regression Rate of Hybrid Rockets, 35th AIAA/ASME/SAE/ASEE Joint Propulsion Conference & Exhibit, (1999), AIAA 99-2323.

The Japan Society of Mechanical Engineers ed., Mechanical Engineering Handbook, Basic Edition α4: Fluid Engineering (2006), pp. 72-73, the Japan Society of Mechanical Engineers (in Japanese).

Usuki, T. and Shimada, T., Improvement on Thrust Profile Flexibility by Oxidizer-to-Fuel Ratio Feedback Control in Hybrid Rocket, 66th International Astronautical Congress (2015), IAC-15, C4, 2, 3.

Waidmann, W., Thrust Modulation in Hybrid Rocket Engines, Journal of Propulsion and Power, Vol. 4, No. 5 (1988), pp. 421-427.

Wernimont, E., J. and Heister, S., D., Progress in Hydrogen Peroxide Oxidized Hybrid Rocket Experiments, 32nd AIAA/ASME/SAE/ASEE Joint Propulsion Conference & Exhibit, (1996), AIAA 96-2696.

[DOI: 10.1299/xxx.2017xxx000x]